Numerical analysis on singular solutions of the Poisson equation in two-dimensions

Z. Yosibash

Abstract A numerical method for extracting the coefficients of the asymptotic series solution of the Poisson equation in two dimensions in the vicinity of singular points is presented. This method is an extension of that presented in (Szabó and Yosibash 1996) to *non-homogeneous boundary value problems*, and is general in the sense that it is applicable to almost any type of point singularity. Numerical experiments for crack-tip singularities, re-entrant corner singularities, abrupt change in boundary conditions, and singularities associated with a multi-material inclusion are presented to substantiate the proposed techniques. Constant as well as varying non-homogeneous "right-hand-side" functions are studied.

1
Introduction
Solutions of two dimensional linear elliptic problems may be singular at a point in one of the following cases: (a) the boundary is unsmooth, (b) the boundary is smooth, but the nature of the boundary conditions change abruptly, or (c) one or more data are unsmooth (an example is the interface point of two domains having different properties). In the vicinity of a singular point the solution is uniquely characterized by an asymptotic series of eigen-functions along with the series coefficients (see e.g. Kondratiev 1967). Determination of the eigen-functions and the associated coefficients is of significant importance because many physical phenomena are correlated to them. In fact, the determination of the first two coefficients (called *stress intensity factors*) in linear elasticity is at the heart of two-dimensional linear fracture mechanics.

The main focus of this paper is the singular part of solutions of the Poisson equation $\nabla^2 u = -f$ which arises, for example, in the Poiseuille flow along a straight duct of cross-section Ω containing re-entrant corners, the Saint Venant torsion of a bar made of two different materials or having an unsmooth cross-section, the deflection of a membrane with a free half-edge, etc. From the operator

Z. Yosibash
Pearlstone Center for Aeronautical Engineering Studies, Dept. of Mechanical Engineering, Ben-Gurion University of the Negev, Beer-Sheva 84105, Israel
E-mail: Zohary@Bgumail.BGU.AC.IL

theory viewpoint, a general approach for Poisson problems over corner domains can be found in (Grisvard 1985; Dauge 1988). The exact solution u of the Poisson equation is analytic in Ω, except in the vicinity of the singular points. In their vicinity the "singular solution" u consists of two parts: $u = u_H + u_P$, where u_H is the homogeneous solution and u_P is the particular solution because of the right hand side "loading" f. Homogenous or periodic boundary conditions in the vicinity of the singular point are considered. The homogeneous solution is given by the asymptotic series:

$$u_H = \sum_{i=1}^{\infty} A_i r^{\alpha_i} f_i(\theta), \quad \alpha_i \le \alpha_{i+1} \ , \tag{1}$$

r and θ being the polar coordinates centered at the singular point. A_i are the coefficients of the asymptotic series, and α_i and $f_i(\theta)$ are the eigenvalues and eigen-functions, which are associated pairs. $f_i(\theta)$ are regular (smooth) functions. The cases when u_H contains $r^{\alpha_i} \ln(r)$ terms, or when the boundaries are curved in the vicinity of the singular point are not addressed herein. The eigen-pairs depend on the coefficients of the partial differential equation, the geometry and the type of boundary conditions in the vicinity of the singular point only, and *are independent of* the loading f. Methods for computing analytically or numerically the eigen-pairs can be found, for example, in (Grisvard 1985; Leguillon and Sanchez-Palencia 1987; Papadakis 1988; Yosibash and Szabó 1995; Costabel and Dauge 1995) and the references therein. Notice that if $\alpha_i < 1$, the corresponding ith term in the expansion (1) for ∇u_H is unbounded as $r \to 0$. We can think of the coefficients A_i of these term as analogous to the stress intensity factors of elasticity, and we denote them by generalized flux intensity factors (GFIFs). The GFIFs are important from the engineering point of view because they are related to failure theories. Although the eigen-pairs of u_H do not depend on the loading, the GFIFs do depend, and *their numerical computation is addressed in this paper.*

For example, consider an isotropic domain with a singular point at the intersection of two straight edges Γ_1 and Γ_2, as shown in Fig. 1, with the following homogeneous boundary conditions:

$$B_i(u) = 0 \quad \text{on } \Gamma_i \quad i = 1, 2 \ . \tag{2}$$

B_i is the trace operator for *Dirichlet boundary conditions*, and $\partial/\partial n$ for *Neumann boundary conditions*, where n denotes the outward normal vector to the boundary. The eigen-pairs of the homogeneous solution (1) for this case
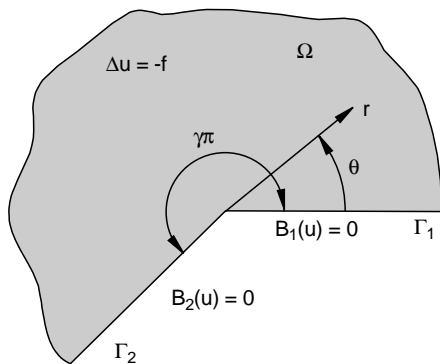
Fig. 1. Domain with a re-entrant corner and notation

are (see Leguillon and Sanchez-Palencia 1987, p. 28 and 40):

For Dirichlet BCs   on Γ_1 and Γ_2

$$\alpha_i = i/\gamma \quad f_i(\theta) = \sqrt{2/(\gamma\pi)} \sin(i\theta/\gamma) \tag{3}$$

For Neumann BCs   on Γ_1 and Γ_2

$$\alpha_i = i/\gamma \quad f_i(\theta) = \cos(i\theta/\gamma) \tag{4}$$

For Dirichlet BCs on Γ_1 and Neumann BCs on Γ_2

$$\alpha_i = i/2\gamma \quad f_i(\theta) = \sqrt{2/(\gamma\pi)} \sin(i\theta/2\gamma) \tag{5}$$

Under mild regularity restriction on f in the vicinity of the singular point, we may expand f in a series of the form:

$$f = \sum_{i=0}^{\infty} r^i \phi_i(\theta) \ . \tag{6}$$

By the shift theorem, the particular solution u_P for the cases that $i + 2 \neq \alpha_j \, \forall i, j$ is:

$$u_P = \sum_{i=0}^{\infty} r^{i+2} \psi_i(\theta) \ . \tag{7}$$

Otherwise, for each α_j which satisfies $i + 2 = \alpha_j$, the series expansion (7) will contain a term of the form

$$r^{i+2}[c_j \ln(r) f_j(\theta) + \psi_i(\theta)] \ , \tag{8}$$

with c_j chosen such that the "Fredholm's Alternative" is satisfied (see Gilbarg and Trudinger 1977, pp. 78–80). It is important to notice that $\psi_i(\theta)$ can be constructed as a linear combination of $f_i(\theta)$ as shown in (Strang and Fix, 1973, chapt. 8).

Many different successful numerical approaches which deal with Poisson problems with singularities have been reported over the years, however, most of these are concerned with the global accuracy of the solution, without considering the explicit computation of the singular series solution. See for example the recent publications (Oh and Babuška 1992; Givoli and Rivkin, 1993) and the references therein. The computation of GFIFs associated with the singular solution to Poisson problem received scant attention in the past, and the *dual singular function method* in (Blum and Dobrowolski 1982) as well as the *generalized influence function method* presented in (Babuška and Miller, 1984) are two of the efficient methods known to the

author, although these are not applicable to multi-material interfaces or anisotropic materials in the form presented in (Blum and Dobrowolski 1982; Babuška and Miller, 1984). Recently, another efficient procedure based on multigrid methods was proposed in (Brenner 1996).

Herein the principle of minimum complementary energy (which is equivalent to the weak complementary principle presented in (Szabó and Yosibash 1996)) is extended for extracting the GFIFs associated with the singular solution of the Poisson problem. The modified Steklov method in (Yosibash and Szabó 1995) is used for computing the eigen-pairs in (1), and the method in (Szabó and Yosibash 1996) together with Richardson extrapolation (Ralston and Rabinowitz 1977 pp. 94–95) are applied for extracting the GFIFs from the finite element solution [the method in (Szabó and Yosibash 1996) is applicable only to Laplace problem, and fails for non-homogeneous problems as the Poisson problem]. This is a finite element post-solution technique applied on a localized sub-domain, enabling a robust, efficient and accurate computation of singular solutions of the Poisson problem.

In Sect. 2 we formulate the techniques for extracting the first series coefficients A_i and the eigen-functions for Poisson problems. Section 3 presents the results of three numerical examples solved by the p-version of the finite element method (Szabó and Babuška 1991), to substantiate the techniques presented in Sect. 2, and the discussion and conclusions are given in Sect. 4. The numerical examples involve constant as well as varying right hand side loadings.

2
Formulation

2.1
Notations and preliminaries

Let $\partial\Omega = \cup_i \Gamma_i$ where Γ_i are analytic simple arc curves called edges. These edges intersect at points called vertices. The two *straight* boundaries which intersect in the singular point will be denoted by Γ_1 and Γ_2. On Γ_1 and Γ_2 we assume homogeneous boundary conditions. On the remaining boundaries we consider Dirichlet boundary conditions $u = \hat{u}$ on Γ_i^D, and Neumann boundary conditions $\frac{du}{dn} = \hat{t}$ on $\partial\Omega - \Gamma_i^D (\Gamma_i^D$ or $\partial\Omega - \Gamma_i^D$ may be $\emptyset)$. We define the space $H_o^1(\Omega) = \{u \in H^1(\Omega) \ u = 0 \text{ on } \Gamma_i^D\}$ where H^1 is the usual Sobolev space. Also, we define the "statically admissible space" (or so-called $H^1(div, \Omega_R)$ space) over a sub-domain Ω_R for a flux vector function, $\boldsymbol{q}$, as follows

$$E_c(\Omega_R) = \left\{(q_1, q_2) \Big| \iint_{\Omega_R} |\boldsymbol{q}|^2 d\Omega < \infty, \ \frac{\partial q_1}{\partial x_1} + \frac{\partial q_2}{\partial x_2} = -f. \right\} , \tag{9}$$

where f is the "loading" in the right hand side of the Poisson equation. When on a part of the boundary of Ω_R, defined by $(\Gamma_R)_q, q_i = 0$, it is necessary to restrict the statically admissible space as follows:

$$\tilde{E}_c(\Omega_R) = \{(q_1, q_2), \ \boldsymbol{q} \in E_c(\Omega_R), \ q_i = 0 \ \text{ on } (\Gamma_R)_q\} \ . \tag{10}$$

Note that if $(q_1, q_2) = \left(\frac{\partial u}{\partial x_1}, \frac{\partial u}{\partial x_2}\right)$, the condition $\frac{\partial q_1}{\partial x_1} + \frac{\partial q_2}{\partial x_2} = -f$ is nothing more than the Poisson equation itself.

In the primal weak formulation, the *exact* solution over the domain Ω is obtained by using the weak form:

Seek $u \in H_o^1(\Omega)$, s.t. $\quad \mathcal{B}(u, v) = \mathcal{F}(v) \quad \forall v \in H_o^1(\Omega)$,

$$(11)$$

where:

$$\mathcal{B}(u, v) = \int_\Omega \sum_{i=1}^2 \frac{\partial u}{\partial x_i} \frac{\partial v}{\partial x_i} \, d\Omega \ ,$$

$$\mathcal{F}(v) = \int_{\partial\Omega - \Gamma^D} \hat{t} v \, ds + \int_\Omega f v \, d\Omega \ . \tag{12}$$

By $\|u\|_E = \sqrt{\mathcal{B}(u, u)}$ we denote the "energy norm" of u. We use the p-version of the finite element method for approximating the solution of the weak form, i.e. we use a hierarchic sequence of finite dimensional spaces $S_1(\Omega) \subset \cdots \subset S_i(\Omega) \subset H_o^1(\Omega)$. The S_i's are linear combination of continuous piecewise polynomials of degree p on the elements of the mesh.

The *approximated* finite element solution to the weak form (11), $u_{FE}^i \in S_i$, is obtained if the infinitely large space $H_o^1(\Omega)$ is replaced by the finite dimensional space S_i. We denote the error in energy norm by $\|e\|_E \stackrel{\text{def}}{=} \|u - u_{FE}^{(i)}\|_E$. Using the p-version of the FEM with the proper (known) mesh refinement towards the singular point, the error in energy norm converges exponentially as the number of degrees of freedom $N(\approx p^2)$ is increased (see Babuška and Suri 1994):

$$\|e\|_E \leq C \exp(-dN^{1/3}) \ , \quad d > 0 \tag{13}$$

where C and d are constants. It has been also shown that in the asymptotic range the estimates are sharp, meaning that the $\leq$ sign may be replaced by "approximately equal" ($\approx$).

2.2
Extracting the series coefficients
The first step in the overall method is obtaining u_{FE} over Ω. This is achieved by the p-version of the FEM using a mesh graded towards the singular point with a pre-known factor (see Szabó and Babuška 1991). In the post-solution phase a circular sector sub-domain Ω_R is considered in the vicinity of the singular point as shown in Fig. 2. We use the principle of minimum complementary energy over Ω_R:
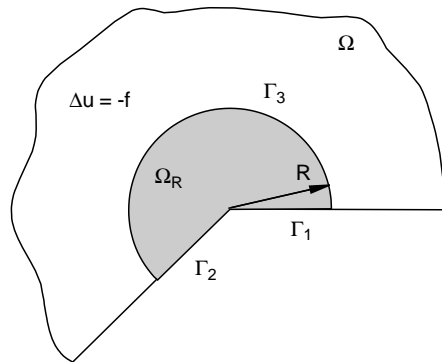

Fig. 2. Extraction sub-domain

Seek $\boldsymbol{q} \in \tilde{E}_c(\Omega_R)$ such that $\mathcal{I}(\boldsymbol{q}) \stackrel{\text{def}}{=} \frac{1}{2}\mathcal{B}_c(\boldsymbol{q}, \boldsymbol{q}) - \mathcal{F}_c(\boldsymbol{q})$ obtains a minimum, $\tag{14}$

where,

$$\mathcal{B}_c(\boldsymbol{q}, \boldsymbol{q}) \equiv \iint_{\Omega_R} \boldsymbol{q}^T \cdot \boldsymbol{q} \, d\Omega = \iint_{\Omega_R} \sum_{i=1}^2 q_i^2 r \, dr \, d\theta \ ,$$

$$(15)$$

and,

$$\mathcal{F}_c(\boldsymbol{q}) \equiv \int_{\partial\Omega_R - (\Gamma_R)_q} \hat{u}(\boldsymbol{q}^T \cdot \boldsymbol{n}) \, ds$$

$$= \int_{\partial\Omega_R - (\Gamma_R)_q} \hat{u}(q_1 \cos\theta + q_2 \sin\theta) \, ds \ . \tag{16}$$

u_{FE} is substituted instead of $\hat{u}$ in (16). Because homogeneous boundary conditions are considered on Γ_1 and Γ_2, the integral in (16) degenerates to integration along Γ_3 alone. One of the most important considerations when applying the principle of minimum complementary energy formulation is the construction of the statically admissible space $\tilde{E}_c(\Omega_R)$. Because the eigen-pairs, which mimic the functional representation of the solution in the neighborhood of singular points, can be computed, we exploit this information for constructing $\tilde{E}_c(\Omega_R)$. This space is spanned by linearly independent flux vectors $\boldsymbol{q}_i$ obtained from the *homogeneous* eigen-pairs and the particular solution $(u = (u_H)_i + u_P)$, i.e.:

$$\sum_{i=1}^\infty A_i \boldsymbol{q}_i + \boldsymbol{q}_P = \sum_{i=1}^\infty A_i \left\{ \begin{matrix} \frac{\partial u_H}{\partial x_1} \\ \frac{\partial u_H}{\partial x_2} \end{matrix} \right\}_i + \left\{ \begin{matrix} \frac{\partial u_P}{\partial x_1} \\ \frac{\partial u_P}{\partial x_2} \end{matrix} \right\}$$

$$= \sum_{i=1}^\infty A_i \left\{ \begin{matrix} \cos\theta \frac{\partial u_H}{\partial r} - \frac{\sin\theta}{r} \frac{\partial u_H}{\partial\theta} \\ \sin\theta \frac{\partial u_H}{\partial r} + \frac{\cos\theta}{r} \frac{\partial u_H}{\partial\theta} \end{matrix} \right\}_i + \left\{ \begin{matrix} \frac{\partial u_P}{\partial x_1} \\ \frac{\partial u_P}{\partial x_2} \end{matrix} \right\} \ . \tag{17}$$

Substituting (1) and (7) into (17) one obtains:

$$\sum_{i=1}^\infty A_i \boldsymbol{q}_i + \boldsymbol{q}_P = \sum_{i=1}^\infty A_i r^{\alpha_i - 1} \left\{ \begin{matrix} \alpha_i \cos\theta f_i(\theta) - \sin\theta f_i'(\theta) \\ \alpha_i \sin\theta f_i(\theta) + \cos\theta f_i'(\theta) \end{matrix} \right\}$$

$$+ \sum_{n=0}^\infty r^{n+1} \left\{ \begin{matrix} (n+2)\cos\theta \psi_n(\theta) - \sin\theta \psi_n'(\theta) \\ (n+2)\sin\theta \psi_n(\theta) + \cos\theta \psi_n'(\theta) \end{matrix} \right\} \ .$$

$$\sum_{i=1}^\infty A_i \boldsymbol{q}_i + \boldsymbol{q}_P = \sum_{i=1}^\infty A_i r^{\alpha_i - 1} \boldsymbol{F}_i(\theta) + \sum_{n=0}^\infty r^{n+1} \boldsymbol{\Psi}_n(\theta) \tag{18}$$

Clearly the flux vectors generated from $(u_H)_i + u_P$ satisfy the Poisson equation. These flux vectors will satisfy also the homogeneous boundary conditions on Γ_1 and/or Γ_2, only if $\boldsymbol{\Psi}_n(\theta)$ are linear combinations of $\boldsymbol{F}_i(\theta)$. Generally, it is possible to construct such $\boldsymbol{\Psi}_n(\theta)$ as shown in (Strang and Fix 1973, chapt. 8).

Remark 1. As will be demonstrated in the following, for extracting the GFIFs, one does not need to actually compute $\boldsymbol{\Psi}_n(\theta)$.

Remark 2. It may seem as if the proposed method for extracting GFIFs resembles the hybrid methods reported for example in (Atluri and Nakagaki 1986; Chow et al. 1995). However, two major differences exist: a) whereas the hybrid

method constructs a special finite element which is assembled in the overall FE mesh, the proposed method is a post-solution superconvergent operation, therefore can be used with any FE solver without having to interfere with the assembly or solution of the FE equations. b) For non-homogeneous problems, as the ones addressed in this paper, using the hybrid elements would require to explicitly find a particular solution and add it to the trial/test spaces – this is a cumbersome and inefficient process. As will be demonstrated in the following, the present method does not need to incorporate the particular solution in the statically admissible space.

The eigen-pairs can be computed explicitly for isotropic domains, or by the modified Steklov method (Yosibash and Szabó 1995) when these are unknown explicitly (for example at a multi-material interface, or anisotropic domains).

We discretize the principle of minimum complementary energy (14) by constructing a finite dimensional subspace of $\tilde{E}_c(\Omega_R)$. This subspace $\tilde{E}_c^N(\Omega_R)$ of dimension N is spanned by a finite number of flux vectors given in (18), i.e. $i = 1, 2, \ldots, N$. Employing the discretized principle of minimum complementary energy one has to consider:

$$\frac{\partial \mathscr{I}(\boldsymbol{q})}{\partial A_i} = 0 \quad i = 1, \ldots, N \ . \tag{19}$$

A system of N equations is obtained, given in a matrix form:

$$[B_c]\{A\} = \{F_c\} - \{D\} \ . \tag{20}$$

Here $\{A\} \overset{\text{def}}{=} (A_1, A_2, \ldots, A_N)^T$ and the elements of the compliance matrix $[B_c]$ are:

$$(B_c)_{ij} = \frac{R^{\alpha_i + \alpha_j}}{\alpha_i + \alpha_j} \int_0^{\gamma\pi} \boldsymbol{F}_i^T(\theta) \cdot \boldsymbol{F}_j(\theta) \mathrm{d}\theta \ . \tag{21}$$

For the Poisson equation in an isotropic domain the functions $\boldsymbol{F}_i(\theta)$ are orthogonal in respect to the integral in (21) (see Szabó and Babuška 1991, Sect. 12.1.2) therefore the compliance matrix is diagonal. The vector $\{D\}$ contains elements of the form:

$$
\begin{aligned}
D_i &= \int_0^R \int_0^{\gamma\pi} r^{\alpha_i - 1} \sum_{n=0}^\infty r^{n+1} \boldsymbol{F}_i^T(\theta) \cdot \boldsymbol{\Psi}_n(\theta) r \mathrm{d}r \mathrm{d}\theta \\
&= \sum_{n=0}^\infty \frac{R^{\alpha_i + n + 2}}{\alpha_i + n + 2} \int_0^{\gamma\pi} \boldsymbol{F}_i^T(\theta) \cdot \boldsymbol{\Psi}_n(\theta) \mathrm{d}\theta \ .
\end{aligned} \tag{22}
$$

The elements of the load vector $\{F_c\}$, which correspond to the linear form $\mathscr{F}_c(\boldsymbol{q})$ are:

$$(F_c)_i = R^{\alpha_i} \int_0^{\gamma\pi} u_{FE}(\theta)(\boldsymbol{F}_i^T(\theta) \cdot n) \mathrm{d}\theta \ . \tag{23}$$

Substituting Eqs. (21), (22) and (23) into (20), and dividing by the diagonal term in the compliance matrix one obtains:

$$
\begin{aligned}
A_i(R) = &R^{-\alpha_i} \frac{2\alpha_i \int_0^{\gamma\pi} u_{FE}(R, \theta)(\boldsymbol{F}_i^T(\theta) \cdot n) \mathrm{d}\theta}{\int_0^{\gamma\pi} |\boldsymbol{F}_i(\theta)|^2 \mathrm{d}\theta} \\
&- \sum_{n=0}^\infty R^{n+2-\alpha_i} \frac{2\alpha_i \int_0^{\gamma\pi} \boldsymbol{F}_i^T(\theta) \cdot \boldsymbol{\Psi}_n(\theta) \mathrm{d}\theta}{(\alpha_i + n + 2) \int_0^{\gamma\pi} |\boldsymbol{F}_i(\theta)|^2 \mathrm{d}\theta} \ .
\end{aligned} \tag{24}
$$

We examine (24) for $R < 1$, as $R \to 0$. As may be noticed only the second sum in (24) represents the particular solution u_P added to the statically admissible space (of course also u_{FE} includes in it the particular solution). We now address the possibility that u_P is not added to the statically admissible space: this will induce an error of the order of the second term in (24). However, as $R \to 0$ the first term in the right hand side is at least two orders of magnitude larger when compared with the second term. The second term in (24) resembles the truncation kind of error in numerical differentiation of functions, and if $n + 2 - \alpha_i > 0$ Richardson extrapolation can be successfully applied to reduce it. This suggests that the second term could be neglected and this will contribute a relative error of an order of magnitude $\mathscr{O}(R^2)$ when computing $A_1(R)$, for example. At the limit $R \to 0$ the second term is negligible, and does not affect the accuracy of the extracted A_i.

The restriction $n + 2 - \alpha_i > 0$, $\forall n$, requires that $2 > \alpha_i$ if the loading is constant, or that $\beta + 2 > \alpha_i$ if the loading is of the form $f = r^\beta \phi(\theta)$. Therefore, only the first terms, associated with the singular eigen-pairs could be extracted using the proposed method.

Thus we consider the following technique for the computation of the GFIFs:

a) Neglect the particular solution u_P when constructing the statically admissible space, then extract $(A_i)_{FE}$ by (24) on a sub-domain of radius R_1 (without considering the second term in the right hand side).

b) Repeat step a) over a sequence of decreasing sub-domains of radii R_j, $R_j < R_{j-1} < \ldots < R_1$.

c) Use Richardson extrapolation (Ralston and Rabinowitz 1977, pp. 94–95) with the error behaving as $R^{2-\alpha_i}$ to extrapolate A_i at the limit $R \to 0$. We can generate a table of A_1s, for example, by the recursive formula:

$$(A_1)_j^{(m)} = (A_1)_{j-1}^{(m+1)} + \frac{(A_1)_{j-1}^{(m+1)} - (A_1)_{j-1}^{(m)}}{(R_j/R_{j+m})^{2-\alpha_1} - 1}$$

and the accuracy of A_1 improves as j and m increase (j corresponds to the radius R_j of the sub-domains Ω_R which is the row number in the generated table, and m corresponds to the column number – see Table 2 for example).

The eigen-pairs used in (24) are computed numerically using the modified Steklov method as described in detail in (Yosibash and Szabó 1995).

Remark 3. In the more general case of the Poisson equation over multimaterial interface domains, or anisotropic domains, the compliance matrix can be fully populated, and an explicit expression for A_i as given in (24) is not obtainable. However, computation of the singular GFIFs by (20) neglecting u_P in the statically admissible space, for several R_js and extrapolating to the limit is still valid due to similar arguments (this will be shown by a numerical example). The mathematical analysis of this case is more cumbersome and is not provided herein.

Remark 4. The loading f may sometimes be given by $\sum_{m=1}^M r^{\beta_m} \phi_m(\theta), \beta_m < \beta_{m+1}$. For any loading with $\beta_1 > -2$

the proposed Richardson extrapolation is valid with an error behaving as $R^{\beta_1 + 2 - \alpha_i}$.

Remark 5. The situation described in (8) will affect the second term in (24), and it seems as the leading term will be of an order of $R^{n+2-\alpha_i}[1 + \ln(R)]$. However, this is not the case due to Fredholm's alternative, and the orthogonality of $\boldsymbol{F}_i$ to the function $\boldsymbol{\Psi}_j$ (associated with the particular solution in (8)) will eliminate the $\ln(R)$ function. This will be shown in the numerical examples.

3
Numerical examples
The analysis presented in the previous section is substantiated by the computation of the first one or two series coefficients $(A_i)_{FE}$ for several Poisson problems of engineering importance for which analytical solutions are available. Results for a new problem, a bi-material inclusion, for which no analytic solution is available, will also be provided. The numerical algorithm is as follows:

(a) Compute the eigenvalues associated with the homogeneous part of the solution, α_i, and the associated eigen-functions, by the modified Steklov method (Yosibash and Szabó 1995). Using the "shift theorem", based on the non-homogeneous "loading", determine the smallest power β_1 of r, associated with the particular solution.
(b) Obtain a finite element solution, u_{FE}, for the problem of interest having a small relative error measured in the energy norm.
(c) Extract the series coefficients $(A_i)_{FE}$ by the principle of minimum complementary energy for several values of integration radii R.
(d) Use Richardson extrapolation with the error behaving as $R^{\beta_1 - \alpha_i}$ to determine the values of $(A_i)_{FE}$ as $R \to 0$.

The numerical solution u_{FE} to all Poisson problems discussed in the following is obtained by means of the p-version finite element computer code Stress Check[*]. The trial spaces used in the finite element analyses is the trunk space (Szabó and Babuška 1991) and the polynomial level of the trial functions is always increased from 1 to 8. In all examples, the integration is performed along a circle of radius R greater than the radius of the elements having a vertex at the singular point. This is because the finite element solution in the first group of elements at the singular point is not of high accuracy.

3.1
Saint Venant torsion of rods
The Saint Venant torsion problem can be formulated in terms of Prantl's stress potential u as follows (see e.g. (Sokolnikoff 1956, Chapter 35)):

$$\nabla^2 u = -2 \quad \text{in } \Omega \tag{25}$$

$$u = 0 \quad \text{on } \partial\Omega . \tag{26}$$
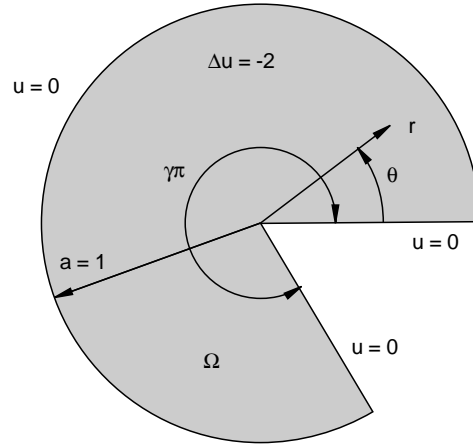
Fig. 3. Cross-section of a rod with a re-entrant corner

The shear stresses are related to the stress potential via:

$$\tau_{x_1 x_3} = \mu k \frac{\partial u}{\partial x_2}, \quad \tau_{x_2 x_3} = -\mu k \frac{\partial u}{\partial x_1} ,$$

where μ is the shear modulus, and k is the angle of twist per unit length of the rod. Poiseuille flow along a straight duct of cross section Ω is described by the same system (25) and (26) where the non-homogeneous term is the applied pressure gradient over the viscosity of the fluid.

Consider a long rod with $\mu k = 1$ and a cross-section in the shape of a circular sector of radius 1, shown in Fig. 3. The exact solution of this problem, $u = u_H + u_P$, is (e.g. (Givoli and Rivkin 1993)[*], (Moffatt and Duffy 1980)):

$$u_H(r, \theta) = \sum_{n=1,3,5,\ldots} \frac{8 a^{2-n/\gamma}}{n\pi[4 - (n/\gamma)^2]} r^{n/\gamma} \sin(n\theta/\gamma) \tag{27}$$

$$= A_1 r^{1/\gamma} \sin(\theta/\gamma) + A_3 r^{3/\gamma} \sin(3\theta/\gamma) + \mathcal{O}(r^{5/\gamma}) \tag{28}$$

$$u_P(r, \theta) = r^2 \sum_{n=1,3,5,\ldots} \frac{8}{n\pi[4 - (n/\gamma)^2]} \sin(n\theta/\gamma),$$
$$\gamma \neq 1/2, 3/2 , \tag{29}$$

$$u_P(r, \theta) = r^2 \frac{-2}{\pi} \left[\frac{\pi}{4} + \ln(r) \cos(2\theta) - \theta \sin(2\theta) \right],$$
$$\gamma = 1/2 . \tag{30}$$

$$u_P(r, \theta) = r^2 \frac{-2}{3\pi} \left[\frac{3\pi}{4} - \ln(r) \cos(2\theta) + \theta \sin(2\theta) \right],$$
$$\gamma = 3/2 . \tag{31}$$

Of great technical importance in fracture mechanics is the "stress intensity factor" defined by $\frac{1}{\gamma} A_1$, thus we extract the first coefficient of the expansion (28). We demonstrate the accuracy of the obtained results on two corner angles $\gamma\pi = 1.5\pi$, and $\gamma\pi = 2\pi$ (a crack in the circular domain). Examining (28) and (29) one observes that:
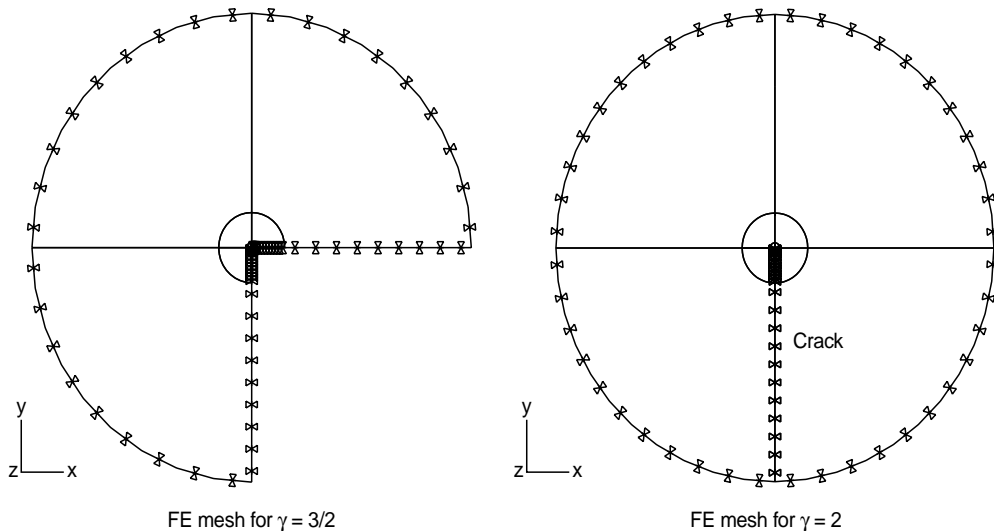
FE mesh for γ = 3/2   FE mesh for γ = 2

Fig. 4. Finite element meshes used for rod torsion problems

For $\gamma = 3/2$ $\quad \beta_1 - \alpha_1 = 2 - 2/3 = 4/3$ (32)

For $\gamma = 2$ $\quad \beta_1 - \alpha_1 = 2 - 1/2 = 3/2$

$$\beta_1 - \alpha_2 = 1/2 \quad (33)$$

The finite element meshes used in the solution domains are presented in Fig. 4. In the vicinity of the singular point the finite element mesh contains two radial layers graded in a geometric progression with the grading factor 0.15. The quality of the finite element solution is summarized in Table 1. As the p-level is increased over the elements, the series coefficients $(A_i)_{FE}$, converge quickly. As an example we show in Fig. 5 the convergence of $(A_1)_{FE}$ for the rod with the cross-section $\gamma = 2$ extracted at $R = 0.5$.

Rod with a crack $(\gamma = 2)$: Extracted values of $(A_1)_{FE}$ and $(A_3)_{FE}$ as $p \to \infty$ for different values of R are listed in Tables 2 and 3 respectively, together with the Richardson extrapolated values as $R \to 0$. By the mathematical analysis, the error in $(A_1)_{FE}$ behaves like $R^{3/2}$ as $R \to 0$, and the error in $(A_3)_{FE}$ behaves like $R^{1/2}$. These powers are used for Richardson extrapolation. Tables 2 and 3 clearly demonstrate that the series coefficients (equivalently the stress intensity factors) are extrapolated with very high accuracies, even though the relative errors at finite values of R are larger than 20% . The significant reduction in the

error already at the first step of Richardson algorithm, and the similarity of the results in each column, strongly support the mathematical analysis.

Rod with a re-entrant corner $(\gamma = 3/2)$: The value of A_1 alone can be extracted in this case because the next term in the series of the homogeneous solution is of the same order as the particular solution. This example also demonstrates that the $\ln(R)$ term does not affect the Richardson extrapolation as noted in Remark 5. Extracted values of $(A_1)_{FE}$ as $p \to \infty$ for different values of R are listed in Table 4, together with the Richardson extrapolated values as $R \to 0$. Here, the mathematical analysis predicts an error behaving like $R^{4/3}$ as $R \to 0$. This power is used for Richardson extrapolation. Again, Table 4 demonstrates that the series coefficients (equivalently the stress intensity factors) are extrapolated with very high accuracies.

Table 1. Convergence of the FE solution for the rod torsion problems

	$\gamma = 3/2$		$\gamma = 2$	
p-level	DOF	Estimated $\|e\|_{E(\Omega)}$ (%)	DOF	Estimated $\|e\|_{E(\Omega)}$ (%)
1	4	68.64	6	63.57
2	16	22.75	23	19.06
3	31	22.24	44	18.04
4	55	9.23	77	7.73
5	88	4.65	122	4.07
6	130	2.46	179	2.34
7	181	1.40	248	1.49
8	241	0.86	329	1.00

360°, Rod in Torsion runs 1 to 8
Generalized Stress Intensity Factors, Int. Radius = 0.5

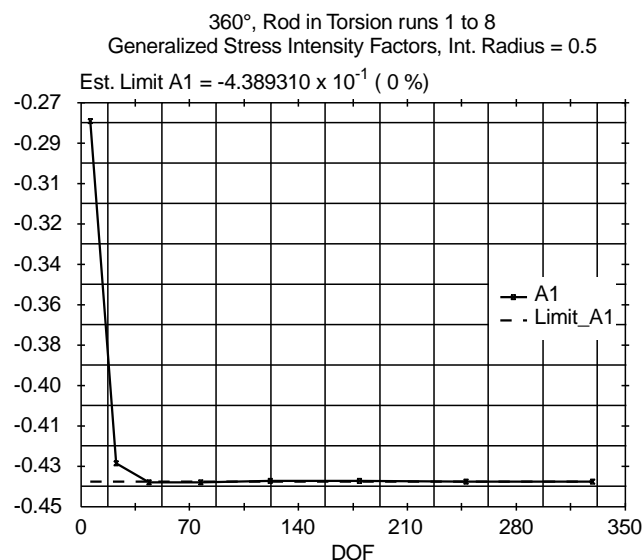Est. Limit A1 = -4.389310 x 10⁻¹ (0 %)

Fig. 5. Convergence of $(A_1)_{FE}$ at $R = 0.5$ for $\gamma = 2$ as the number of DOF increases

Table 2. $(A_1)_{FE}$ at various values of R for the rod problem with a crack ($\gamma = 2$) and the extrapolated values as $R \to 0$ (The numbers in the parentheses represent the relative error. $(A_1)_{EX} = 0.6790611$)

R	$(A_1)_{FE} \overset{\text{def}}{=} A_1^{(0)}$	$A_1^{(1)}$	$A_1^{(2)}$
0.5	0.4389309882 (−35.4%)		
		0.6786281319 (−0.064%)	
0.1	0.6571889676 (−3.22%)		0.6779644845 (−0.16%)
		0.6779854708 (−0.158%)	
0.05	0.6706327966 (−1.24%)		

Table 3. $(A_3)_{FE}$ at various values of R for the rod problem with a crack ($\gamma = 2$) and the extrapolated values as $R \to 0$ (The numbers in the parentheses represent the relative error. $(A_3)_{EX} = 0.48504364$)

R	$(A_3)_{FE} \overset{\text{def}}{=} A_3^{(0)}$	$A_3^{(1)}$	$A_3^{(2)}$
0.5	0.1420192005 (−70.7%)		
		0.4848862574 (−0.032%)	
0.1	0.3315514481 (−31.6%)		0.4865664859 (0.32%)
		0.4860351510 (−0.204%)	
0.05	0.3767986771 (−22.3%)		

Table 4. $(A_1)_{FE}$ at various values of R for the rod problem with a re-entrant corner ($\gamma = 3/2$) and the extrapolated values as $R \to 0$ (The numbers in the parentheses represent the relative error. $(A_1)_{EX} = 0.71619725$)

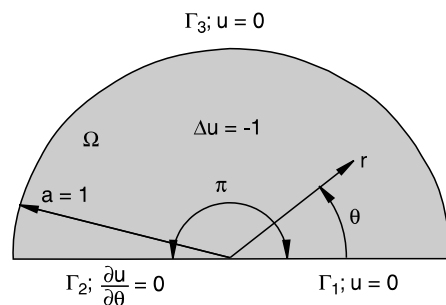| R	$(A_1)_{FE} \overset{\text{def}}{=} A_1^{(0)}$	$A_1^{(1)}$	$A_1^{(2)}$
0.5	0.4319778445 (−39.7%)		
		0.7161427486 (−0.008%)	
0.1	0.6829066198 (−4.65%)		0.7160281039 (−0.24%)
		0.7160334253 (−0.023%)	
0.05	0.7028870438 (−1.86%)		

3.2
Semicircular membrane with a free half-edge
It is well known that the point at which the boundary conditions change abruptly, is singular. This example problem treats the so-called Motz's problem, however, unlike the classical formulation where the Laplace equation is considered, our interest is in the Poisson equation. Consider a semicircular domain shown in Fig. 6. The solution of the following problem is of interest:

$$\nabla^2 u = -1 \quad \text{in } \Omega \tag{34}$$

$$u = 0 \quad \text{on } \Gamma_1 \cup \Gamma_2 \tag{35}$$

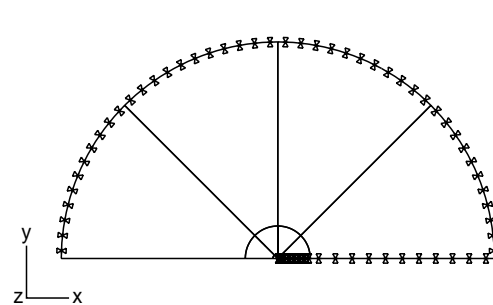$$\frac{\partial u}{\partial n} = \frac{\partial u}{\partial \theta} = 0 \quad \text{on } \Gamma_3 . \tag{36}$$

The exact solution in the vicinity of the singular point is given in (Babuška and Miller 1984):

$$u(r, \theta) = A_1 r^{1/2} \sin \theta/2 + A_2 r^{3/2} \sin 3\theta/2 + \mathcal{O}(r^2) , \tag{37}$$

where the first two terms correspond to the homogeneous part of the solution, the particular solution is of order $\mathcal{O}(r^2)$ and $(A_1)_{EX} = 0.339531$, $(A_2)_{EX} = 0.242522$. In this example problem it is seen that the error in $(A_1)_{FE}$ approaches zero at a rate $R^{3/2}$ and the error in $(A_2)_{FE}$ approaches zero at a rate $R^{1/2}$. The finite element mesh used for this example problem is shown in Fig. 7, having same refinement layers as previously explained. The quality of the finite element solution is summarized in Table 5. Extracted values of $(A_1)_{FE}$ and $(A_2)_{FE}$ as $p \to \infty$ for different

Fig. 6. Semicircular membrane with a free half-edge – Domain and boundary conditions

Fig. 7. Finite element mesh used for the semicircular membrane with a free half-edge

Table 5. Convergence of the FE solution for the semicircular membrane with a free half-edge

p-level	1	2	3	4	5	6	7	8
DOF	8	28	52	88	136	196	268	352
Est.$\|e\|_{E(\Omega)}$ (%)	61.97	12.10	10.39	4.66	2.46	1.58	1.14	0.86

Table 6. $(A_1)_{FE}$ at various values of R for the semicircular membrane with a free half-edge, and the extrapolated values as $R \to 0$ (The numbers in the parentheses represent the relative error. $(A_1)_{EX} = 0.339531$)

R	$(A_1)_{FE} \overset{\text{def}}{=} A_1^{(0)}$	$A_1^{(1)}$	$A_1^{(2)}$
0.5	0.2194689364 (−35.4%)		
		0.3393546788 (−0.052%)	
0.1	0.3286317720 (−3.22%)		0.3390853374 (−0.131%)
		0.3390938547 (−0.129%)	
0.05	0.3353949499 (−1.22%)		

Table 7. $(A_2)_{FE}$ at various values of R for the semicircular membrane with a free half-edge, and the extrapolated values as $R \to 0$ (The numbers in the parentheses represent the relative error. $(A_2)_{EX} = 0.242522$)

R	$(A_2)_{FE} \overset{\text{def}}{=} A_2^{(0)}$	$A_2^{(1)}$	$A_2^{(2)}$
0.5	0.0710301494 (−70.7%)		
		0.2425491818 (0.011%)	
0.1	0.1658435386 (−31.6%)		0.2424089315 (−0.0466%)
		0.2424532826 (−0.028%)	
0.05	0.1882820131 (−22.4%)		

values of R are listed in Tables 6 and 7 respectively, together with the Richardson extrapolated values as $R \to 0$. Tables 6 and 7 present a picture very similar to that of the corresponding Tables 2, 3 and 4 of the previous example problem. Again one may notice the high accuracies achieved by the extrapolation algorithm.

$(A_2)_{FE}$ in this example problem and $(A_3)_{FE}$ in the previous example problem are markedly less accurate when extracted at a given radius R, when compared with the corresponding approximations $(A_1)_{FE}$. The errors are related to the term proportional to $R^{\beta_1 - \alpha_i}$. For A_1, the value $\beta_1 - \alpha_1$ is larger than $\beta_1 - \alpha_2$, and since $R < 1$, the error in A_1 is smaller. However, the extrapolation algorithm provides an excellent approximation to the exact value for both $(A_1)_{FE}$ and $(A_2)_{FE}$, regardless of the error at given Rs.

Extraction of A_i at the smallest integration radius $R = 0.05$ is the least accurate because the integration path is the closest to the first layer of elements surrounding the singular point (which have the outer radius equal to $0.15^2 = 0.0225$, therefore contains the largest *numerical error*. One may gain further accuracy by adding an additional layer of elements of an outer radius $0.15^3 = 0.003375$. Numerical experiments support last statement.

The performance of the proposed algorithm for low accuracy finite element solutions is being addressed in the following. One may argue that the true performance must be justified by considering, for example, the finite element solution at p-level = 4, with a relatively large error in energy norm $\|e\|_E = 4.66\%$. Doing so, we present in Tables 8 and 9 same information as in Tables 6 and 7, only that now $(A_1)_{FE}$ and $(A_2)_{FE}$ are extracted at p-level = 4. Comparing Table 8 with 6, and Table 9 with 7 one notices that although the finite element error is 4.66%, yet the extrapolated values of $(A_1)_{FE}$ and $(A_2)_{FE}$ are not sensitive and are provided with an accuracy of about 1%. This is because of the super-convergent property of the extraction procedure for $(A_i)_{FE}$.

3.3
Bi-material inclusion

Two-dimensional bodies consisting of two or more materials perfectly bonded along all their common edges attracted scant attention in the past. Lately, with the growing interest in electronic packaging and composite materials, more attention is focused on the solution to these problems.

Table 8. $(A_1)_{FE}$ at various values of R extracted at p = 4, for the semicircular membrane with a free half-edge, and the extrapolated values as $R \to 0$. (The numbers in the parentheses represent the relative error. $(A_1)_{EX} = 0.339531$)

R	$(A_1)_{FE} \overset{\text{def}}{=} A_1^{(0)}$	$A_1^{(1)}$	$A_1^{(2)}$
0.5	0.2196941098 (−35.29%)		
		0.3385821606 (−0.279%)	
0.1	0.3279484901 (−3.41%)		0.3376024682 (−0.568%)
		0.3376334488 (−0.559%)	
0.05	0.3342092988 (−1.57%)		

Table 9. $(A_2)_{FE}$ at various values of R extracted at p = 4, for the semicircular membrane with a free half-edge, and the extrapolated values as $R \to 0$ (The numbers in the parentheses represent the relative error. $(A_2)_{EX} = 0.242522$)

R	$(A_2)_{FE} \overset{\text{def}}{=} A_2^{(0)}$	$A_2^{(1)}$	$A_2^{(2)}$
0.5	0.0711686231 (−70.6%)		
		0.2394924381 (−1.25%)	
0.1	0.1642157396 (−32.3%)		0.2464274901 (1.6%)
		0.2442344341 (0.71%)	
0.05	0.1876526726 (−22.6%)		

Let $\Omega = \{(r, \theta) : r \le 2, 0 \le \theta \le 2\pi\}$ and let Ω_i be the two sub-domains of Ω occupying the sectors $0 \le \theta \le \pi/2$, and $\pi/2 \le \theta \le 2\pi$. See Figure 8. We conisder the inclusion problem with two kinds of loadings: constant loading $f = 1$ and variable loading $f = \sqrt{r}$.

Constant Loading: Consider the following constant loading problem:

$$p_i \nabla^2 u = -1 \qquad \text{in } \Omega_i \ , \tag{38}$$

with $p_1 = 10$ and $p_2 = 1$, and the following Dirichlet boundary conditions:

$$u = 0 \qquad \text{on } \partial\Omega \ . \tag{39}$$

The unique solution to this inclusion problem is given by (Kellogg 1975):

$$u(r, \theta) = A_1 \, r^{\alpha_1} h_1(\theta) + A_2 \, r^{\alpha_2} h_2(\theta) + \mathcal{O}(r^2) \tag{40}$$

where A_1 and A_2 are unknowns, and

$$\alpha_1 = 0.731691779, \qquad \alpha_2 = 1.268308221 \tag{41}$$

$$h_1(\theta) = \begin{cases} \cos[(1-a)\theta] + c_1 \sin[(1-a)\theta] \\ \qquad\qquad 0 \le \theta \le \pi/2, \\ c_1 \cos[(1-a)\theta] + c_2 c_3 \sin[(1-a]\theta] \\ \qquad\qquad \pi/2 \le \theta \le 2\pi \ , \end{cases} \tag{42}$$
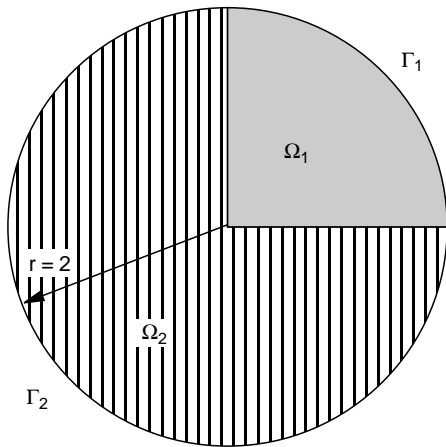
$$h_2(\theta) = \begin{cases} \cos[(1+a)\theta] - c_3 \sin[(1+a)\theta] \\ \qquad\qquad 0 \le \theta \le \pi/2, \\ c_1 \cos[(1+a)\theta] - c_2 c_3 \sin[(1+a]\theta] \\ \qquad\qquad \pi/2 \le \theta \le 2\pi \ , \end{cases} \tag{43}$$

$c_1 = 6.31818181818182$, $c_2 = -2.68181818181818$, $c_3 = 0.64757612580273$, and $a = 0.26830822130025$.
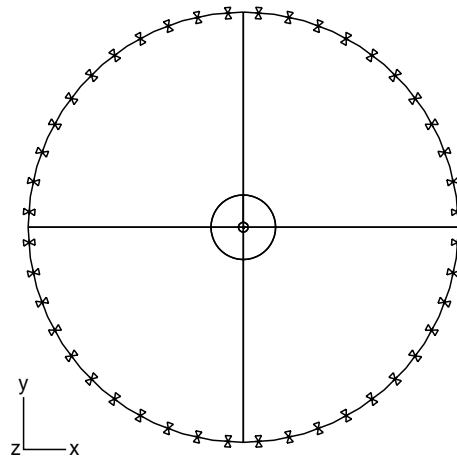
The finite element mesh used in the solution domains are presented in Fig. 9. In the vicinity of the singular point the finite element mesh contains three radial layers, the smallest being of radius 0.003375. The quality of the finite element solution is summarized in Table 10. The extracted value of $(A_2)_{FE}$ is identically zero for all Rs and for all p-levels. The values of $(A_1)_{FE}$ as $p \to \infty$ for different values of R are listed in Table 11 together with the Richardson extrapolated values as $R \to 0$. Based on Table 11 we may conclude with a high level of confidence that $A_1 = 0.040940$ and $A_2 = 0$, and these values being accurate to the sixth significant digit.

Varying Loading: Consider the same problem as in (38) only that the loading is varying:

$$p_i \nabla^2 u = -\sqrt{r} \qquad \text{in } \Omega_i \ , \tag{44}$$

Fig. 8. Bi-material inclusion

Fig. 9. Finite element mesh used for the bi-material inclusion problem

Table 10. Convergence of the FE solution for the bi-material inclusion problem with constant loading

p-level	1	2	3	4	5	6	7	8
DOF	13	53	121	217	341	493	673	881
Est.$\|e\|_{E(\Omega)}$ (%)	51.36	7.14	2.56	0.98	0.48	0.24	0.15	0.10

Table 11. $(A_1)_{FE}$ at various values of R for the bi-material inclusion problem with constant loading, and the extrapolated values as $R \to 0$

R	$(A_1)_{FE} \overset{\text{def}}{=} A_1^{(0)}$	$A_1^{(1)}$	$A_1^{(2)}$	$A_1^{(3)}$
0.5	0.23945084			
		0.040941240		
0.1	0.038734042		0.040940488	
		0.040940529		0.040940036
0.05	0.040024514		0.040940040	
		0.040940066		
0.01	0.040821168			

Table 12. Convergence of the FE solution for the bi-material inclusion problem with varying loading

p-level	1	2	3	4	5	6	7	8
DOF	13	53	121	217	341	493	673	881
Est.$\|e\|_{E(\Omega)}$ (%)	59.26	9.19	3.08	1.23	0.62	0.32	0.20	0.14

Table 13. $(A_1)_{FE}$ at various values of R for the bi-material inclusion problem with varying loading, and the extrapolated values as $R \to 0$

R	$(A_1)_{FE} \overset{\text{def}}{=} A_1^{(0)}$	$A_1^{(1)}$	$A_1^{(2)}$	$A_1^{(3)}$
0.8	0.080927827			
		0.248213515		
0.5	0.175349788		0.248209673	
		0.248209771		0.248205947
0.1	0.243978280		0.248205974	
		0.248206039		
0.05	0.246964970			

Same finite element mesh as shown in Fig. 9 is used, and the quality of the finite element solution is summarized in Table 12.

As before, the extracted value of $(A_2)_{FE}$ is identically zero for all Rs and for all p-levels. The values of $(A_1)_{FE}$ as $p \to \infty$ for different values of R are listed in Table 13. For this problem, the exponent of the varying load is given by $\beta_1 = 0.5$, therefore we use Richardson extrapolation with the error behaving as $\beta_1 + 2 - \alpha_1 = 1.76831$. The extrapolated values of A_1 as $R \to 0$ are summarized in Table 13. Based on Table 13 we may conclude with a high level of confidence that $A_1 = 0.248206$ and $A_2 = 0$, and these values being accurate to the sixth significant digit.

4
Discussion and conclusions

This paper presents a numerical method for extracting the coefficients of the asymptotic series solution of the Poisson equation in two dimensions in the vicinity of singular points. The method, based on the modified Steklov formulation for computing the eigen-pairs, the principle of minimum complementary energy, Richardson extrapolation and the p-version of the finite element method, is shown to be accurate, efficient and robust. Most importantly, the method is applicable to singularities associated with re-entrant corners, abrupt change in boundary conditions, multi-material inclusions and anisotropic materials.

An important step in the development of the overall technique is understanding the structure of the singular particular solution u_P (due to the loading f), and its influence on the GFIFs. The recognition of the behavior of the error in computing the GFIFs when u_P is not included

in the statically admissible space enabled a simplified approach for extracting the GFIFs in a limiting process. Otherwise, one had to explicitly compute u_P and add it to the statically admissible space, resulting in a complicated and cumbersome numerical procedure.

Numerical experiments for crack-tip singularities, re-entrant corner singularities, abrupt change in boundary conditions, and singularities associated with multi-material inclusions are presented. All experiments demonstrate that very accurate GFIFs can be extracted (relative errors within less than 0.5% in most cases), although the integration radii are large and away from the singular point. Thus, a strong mesh refinement in the vicinity of the singular point is unnecessary for obtaining excellent results, enabling an efficient numerical procedure.

References

Atluri, S. N.; Nakagaki, M. (1986): Computational methods for plane problems of fracture. In: Atluri, S. N. (ed). Computational methods in the mechanics of fracture, Amsterdam. Elsevier, pp. 169–227

Babuška, I.; Miller, A. (1984): The post-processing approach in the finite element method – Part 2: The calculation of stress intensity factors. Int. J. Num. Meth. Eng. 20, 1111–1129

Babuška, I.; Suri, M. (1994): The p and h-p versions of the finite element method, basic principles and properties. SIAM review 36 (4), 578–632

Blum, H.; Dobrowolski, M. (1982): On finite element methods for elliptic equations on domains with corners. Computing 28, 53–63

Brenner, C. S. (1996): Multigrid methods for the computation of singular solutions and stress intensity factors I: Corner singularities. Math Comput. (submitted)

Chow, W. T.; Beom, H. G.; Atluri, S. N. (1995): Calculation of stress intensity factors for an interfacial crack between dissimilar

anisotropic media, using a hybrid element and the mutual integral. Comp. Mech. 15, 546–557

Costabel, M.; Dauge, M. (1995): Computation of corner singularities in linear elasticity. In: Costabel, M.; Dauge, M.; Nicaise, S.; (eds.): Boundary value problems and integral equations in nonsmooth domains, Marcel Dekker, New York, Basel, Hong-Kong, 59–68

Dauge, M. (1988): Elliptic boundary value problems in corner domains – smoothness and asymptotics of solutions. Lect Notes Math 1341, Springer-Verlag, Heidelberg

Gilbarg, D.; Trudinger, N. S. (1977): Elliptic partial differential equations of second order. Springer-Verlag, Berlin, Heidelberg, New York

Givoli, D.; Rivkin, L. (1993): The DtN finite element method for elastic domains with cracks and re-entrant corners. Comp. Struct. 49, 633–642

Grisvard, P. (1985): Elliptic problems in nonsmooth domains. Pitman Publishing, England

Kellogg, R. B. (1975): On the Poisson equation with intersecting interfaces. Appl. Anal. 4, 101–129

Kondratiev, V. A. (1967): Boundary value problems for elliptic equations in domains with conical or angular points. Transact. Moscow Math. Soc. 16, 227–313

Leguillon, D.; Sanchez-Palencia, E. (1987): Computation of singular solutions in elliptic problems and elasticity. John Willey & Sons, New York

Moffatt, H. K.; Duffy, B. R. (1980): Local similarity solutions and their limitations. J. Fluid Mech. 96, 299–313

Oh, H.-S.; Babuška, I. (1992): P-version of the element method for the elliptic boundary value problems with interfaces. Comput. Meth. Appl. Mech. Eng. 97 (2), 211–231

Papadakis, P. (1988): Computational aspects of the determination of the stress intensity factors for two-dimensional elasticity. PhD thesis, University of Maryland at College Park, College Park, Maryland, USA

Ralston, A.; Rabinowitz, P. (1977): A first course in numerical analysis. McGraw-Hill, New-York, USA, 2nd edition

Sokolnikoff, I. S. (1956): Mathematical Theory of Elasticity. Mc-Graw-Hill, New York

Strang, G.; Fix, G. J. (1973): An analysis of the finite element method. Prentice-Hall, N.J

Szabó, B. A.; Babuška, I. (1991): Finite Element Analysis. John Wiley & Sons, New York

Szabó, B. A.; Yosibash, Z. (1996): Numerical analysis of singularities in two-dimensions. Part 2: Computation of the generalized flux/stress intensity factors. Int. J. Num. Meth. Eng. 39 (3), 409–434

Yosibash, Z.; Szabó, B. A. (1995): Numerical analysis of singularities in two-dimensions. Part 1: Computation of eigenpairs. Int. J. Num. Meth. Eng. 38 (12), 2055–2082